

# Spatially Varying Small-strain Stiffness in Soils Subjected to $K_0$ Loading

Hyun-Ki Kim\* and J. Carlos Santamarina\*\*

Received July 16, 2015/Revised March 20, 2017/Accepted May 17, 2017/Published Online August 15, 2017

## Abstract

Grain-scale characteristics and formation history determine spatial variability in granular masses. We investigate the effect of spatially varying stiffness on the load-deformation response under zero-lateral strain conditions using numerical simulations of correlated random fields, where the granular medium is represented by a non-linear stress-dependent meso-scale model. Results show that stiffness heterogeneity results in higher global compressibility as compared to the homogeneous medium with the same arithmetic mean stiffness. Furthermore, the non-homogeneous stress field that develops inside the granular mass is characterized by focused load transfer along columnar regions, higher stress anisotropy and lower horizontal-to-vertical stress ratio  $K_0$  than in a granular medium of homogenous stiffness. As the applied stress increases, the inherent stress-dependent response of the granular material leads to a more homogenous stress field. While greater variance in stiffness causes lower global stiffness, a longer correlation length results in greater variance in global mechanical response among multiple realizations.

Keywords: *spatial variability, effective stiffness,  $K_0$  coefficient, uniaxial compaction, zero-lateral strain loading*

## 1. Introduction

Grain-scale characteristics and formation history determine spatial variability in granular masses. Spatial variability can be captured in statistical parameters such as the coefficient of variation and the correlation length (Vanmarcke, 1977; Phoon and Kulhawy, 1999). The coefficient of variation  $COV[\cdot]$  is defined as the ratio of the standard deviation  $\sigma[\cdot]$  to the mean value  $\mu[\cdot]$ . The correlation length  $L[\cdot]$  is the distance where the spatial autocorrelation of a given physicochemical property decays by  $1/e$ , and it indicates the spatial scale of material heterogeneity.

Spatial variability prevails in granular materials at all scales. For example, spatial variability in natural sediments is readily observed in field data (Tang, 1979; Harr, 1987; Ravi, 1992; Kulhawy, 1992; DeGroot and Beacher, 1993; Lacasse and Nadim, 1996; Hegazy *et al.*, 1996), as well as in laboratory-scale studies (Antonellini *et al.*, 1994; Jang *et al.*, 1999; Antonellini *et al.*, 1994; Cho *et al.*, 2004). Typical ranges for the coefficient of variation  $COV$  and the correlation length  $L$  for the properties of natural sediments can be found in previous studies (Phoon and Kulhawy, 1999; Harr, 1987; Lacasse and Nadim, 1996; DeGroot, 1996; Jones *et al.*, 2002).

Probabilistic studies of deformation in heterogeneous soils have often modeled the soil mass as an isotropic linear elastic material with a spatially varying Young's modulus  $E$  (Harr, 1987;

Resendiz and Herrera, 1969; Ang and Tang, 1975; Cambou, 1975; Beacher and Ingra, 1981; Zeitoun and Baker, 1992; Paice *et al.*, 1996; Fenton and Griffith, 2005; Jimenez and Sitar, 2009; Griffith and Fenton, 2009). The following observations can be extracted from these studies:

- The expected elastic deformation increases with increasing coefficient of variation in Young's modulus,  $COV[E]$ .
- The uncertainty in vertical displacement is much more sensitive to Young's modulus variability than to Poisson's ratio variability.
- The variability in computed deformations is negligible when the correlation length  $L$  is much shorter than the specimen size  $D$  ( $D \gg L$ ). However, as the correlation length increases, the variance of the expected deformation also increases.

Linear models fail to capture the inherent non-linear and non-elastic response of granular materials. Consequently, some recent studies have incorporated non-linear elasto-plastic material models to assess settlement and consolidation processes in heterogeneous soils by taking into consideration various spatial scales and anisotropy effects (Niemunius *et al.*, 2005; Suchomel and Masin, 2011; Wu *et al.*, 2011; Huang *et al.*, 2010).

It is also required to be pointed out that significant developments in geomechanics based on micromechanics took place using the Discrete Element Method (DEM) and experimental methods: Force chain formation and networking with anisotropic stress state through particle contacts and graphical representations

\*Member, Associate Professor, School of Civil & Environmental Engineering, Kookmin University, Seoul 02707, Korea (Corresponding Author, E-mail: geotech@kookmin.ac.kr)

\*\*Professor, Dept. of Earth Science and Engineering, King Abdullah University of Science and Technology (KAUST), Saudi Arabia (E-mail: carlos.santamarina@kaust.edu.sa)

(Cundall and Strack, 1979; Rothenburg and Bathurst, 1989; Radjai *et al.*, 1998; Díaz-Rodríguez, and Santamarina, 1999; Oda *et al.*, 2004; Majmudar and Behringer, 2005; Muthuswamy and Tordesillas, 2006; Behringer *et al.*, 2008; Arévalo *et al.*, 2009; Peña *et al.*, 2009; Tordesillas *et al.*, 2010; Barreto and O’Sullivan, 2012; Hurley *et al.*, 2014).

The purpose of this study is to investigate the effects of spatial variability on the load-deformation soil response under zero-lateral strain boundary conditions using the finite element scheme. The stress-dependent non-linear material model and the representation of spatial variability are described first.

## 2. Methodology: Numerical Simulation-material Model

The research is implemented using the finite element program ABAQUS 6.12. In all cases, we simulate a stress-controlled, zero-lateral strain compression test. The square specimen consists of a  $100 \times 100$  mesh made of four-node plane strain elements. Zero horizontal displacement and zero friction conditions are imposed on lateral boundaries. The top and bottom plates are rigid but

free to move in the vertical direction. Simulation details are summarized in Table 1.

Given the added complexity of spatial variability, the rather simple but robust Duncan-Chang material model is selected to represent the nonlinear stress-strain response of the granular mass (Duncan and Chang, 1970). The model is modified to capture the stress-dependent small-strain shear modulus  $G_0$  [kPa] as follows:

$$G_0 = \alpha \left( \frac{\sigma_0}{1 \text{ kPa}} \right)^\beta \quad (1)$$

where  $\sigma_0$  [kPa] is the mean in-plane principal stress  $\sigma_0 = (\sigma_x + \sigma_z)/2$ , the  $\alpha$ -coefficient is the small-strain shear modulus at  $\sigma_0 = 1$  kPa, and the  $\beta$ -exponent captures the stress-sensitivity of the stiffness. Parameters  $\alpha$  [kPa] and  $\beta$  [-] are correlated in natural granular materials (Fernandez, 2000; Santamarina *et al.* 2001):

$$\beta \approx 0.72 - \frac{\sqrt{\alpha} \rho}{350 \text{ m/s}} \quad (2)$$

where  $\rho$  [ton/m<sup>3</sup>] is mass density.

Table 1. Numerical Study: Model, Material Parameters, and Parametric Study

Boundary conditions (all cases):			
<ul style="list-style-type: none"> <li>• Stress controlled vertical z-compression</li> <li>• Zero-lateral global displacement: <math>\epsilon_x = \epsilon_y = 0</math> (y-axis: out-of-plane direction)</li> <li>• No friction against the lateral x and y boundaries</li> <li>• Element type: 4-node plane strain element</li> <li>• Mesh: 100 by 100 elements</li> </ul>			
Duncan-Chang model parameters:			
• Mean value of small-strain shear modulus at 1 kPa		$\alpha = 10^4$ kPa	
• Stress exponent of small-strain shear and bulk moduli		$\beta = 0.49$ (for $\alpha = 10^4$ kPa)	
• Poisson’s ratio at 1 kPa		$\nu_{ikPa} = 0.3$	
• Soil friction angle		$\phi = 30^\circ$	
• Mass density		$\rho = 1.6$ t/m <sup>3</sup>	
• Failure ratio		$R_f = 0.9$	
Random variable and marginal distribution:			
• Small-strain shear modulus at 1 kPa $\alpha$ . Uniform distribution.			
• For each value of $a$ , the corresponding value of $\beta$ is estimated as $\beta \approx 0.72 - \frac{\sqrt{\alpha} \rho}{350 \text{ m/s}}$			
Cases reported in this manuscript:			
Goal of parametric study	Random variability	Relative correlation length L/D	Fig #
Stress-induced homogenization	COV[ $\alpha$ ] = 0.3	0.1	1
		0.02, 0.04, 0.08, 0.1, 0.14, 0.2	2
Stress focusing	COV[ $\alpha$ ] = 0.1, 0.3, 0.5	0.1	3
Variability effects on stress focusing	COV[ $\alpha$ ] = 0, 0.1, 0.2, 0.3, 0.4, 0.5	~0	4a
Correlation length effects on stress focusing	COV[ $\alpha$ ] = 0.3	~0, 0.04, 0.06, 0.1, 0.14, 0.2	4b
Variability effects on $K_0$	COV[ $\alpha$ ] = 0, 0.1, 0.2, 0.3, 0.4, 0.5	~0	5a
Correlation length effects on $K_0$	COV[ $\alpha$ ] = 0.3	~0, 0.04, 0.06, 0.1, 0.14, 0.2	5b
Variability effects on load-deformation	COV[ $\alpha$ ] = 0, 0.1, 0.3, 0.5	~0	6
Variability effects on compressibility	COV[ $\alpha$ ] = 0.1, 0.3, 0.5	0.04, 0.2	7

The  $\alpha$ -coefficient (i.e.,  $G_0$  at  $\sigma_0 = 1$  kPa) is selected as the random variable. This is positively-valued quantity and it is modeled using a bounded uniform distribution with mean  $\mu[\alpha] = 10^4$  kPa to represent a medium density silt or sand (Table 1 summarizes all the material parameters involved in this study). A realization of the granular mass includes both stiffer and softer sediments depending on  $\text{COV}[\alpha]$ ; realizations with the highest  $\text{COV}[\alpha] = 0.5$  correspond to highly heterogeneous soil conditions.

The correlated random field for the small-strain shear modulus parameter  $\alpha$  is generated as follows. Its derivation and details are found in Fenton (1994), El-Kadi and Williams (2000), Vio *et al.* (2001), Fenton and Griffiths (2008):

- (1) Create the covariance matrix  $\underline{\underline{A}}$  [NxN] where N is the number of elements in the finite element mesh. The  $i$ -th row in  $\underline{\underline{A}}$  captures the correlation between the  $i$ -th element and all other elements in the FEM mesh. In particular, the  $A_{ij}$  entry is computed in terms of the pre-selected values for standard deviation  $\sigma$ , correlation length  $L$  and the distance  $d_{ij}$  between mesh elements  $i$  and  $j$ :

$$A_{ij} = \sigma^2 e^{-\frac{1}{L}|d_{ij}|} \quad (3)$$

- (2) Use the matrix decomposition technique to extract the  $\underline{\underline{C}}$  [NxN] matrix from the  $\underline{\underline{A}}$  matrix (El-Kadi and Williams, 2000),

$$\underline{\underline{A}} = \underline{\underline{C}}\underline{\underline{C}}^T \quad (4)$$

- (3) Compute the spatially correlated Gaussian random field  $\underline{X}$  [Nx1]

$$\underline{X} = \underline{\underline{C}} \cdot \underline{\varepsilon} + \underline{T} \quad (5)$$

where the  $i$ -th entry in the vector  $\underline{T}$  [Nx1] is the mean value of the  $\alpha$ -factor for the  $i$ -th element in the mesh; for simulations presented in this paper, all entries in  $\underline{T}$  are equal to  $T_i = \mu[\alpha] = 10$  MPa. The  $\underline{\varepsilon}$  [Nx1] vector is an array of uncorrelated, Gaussian distributed random numbers of zero mean and unit variance.

- (4) Map the generated Gaussian random field onto the uniform distribution adopted from  $\alpha$  in this study. This mapping consist of adopting values with the same cumulative probability (Grigoriu, 1984; Yamazaki and Shinozuka, 1988): We sort all values in  $\underline{X}$  and determine the cumulative probability  $F_G(X_i)$ ; then, for each  $X_i$  value in  $\underline{X}$ , we identify the uniformly distributed value  $a_i$  that has the same cumulative probability  $F_U(a_i) = F_G(X_i)$

$$X_i \rightarrow F_G(X_i) = F_U(a_i) \rightarrow a_i \quad (6)$$

This procedure is repeated to create multiple realizations for each set of parameters, i.e.,  $\text{COV}[\alpha]$  and correlation length  $L[\alpha]$ . Note that there are two length scales in each realization: the specimen size  $D$  and the internal scale of heterogeneity  $L$ . We considered them together, in terms of the relative correlation length  $L/D$ . We limited the relative correlation length to  $L/D \leq 0.2$  to minimize boundary and scaling effects.

According to the previous studies including Ching and Phoon (2013); Song *et al.* (2011), Santoso *et al.* (2011); Huang and Griffiths (2015); Paice *et al.* (1996); Griffiths and Fenton, (2009), etc., autocorrelation characteristics of the geotechnical spatial variability can affect the mechanical responses significantly, which is required to be interpreted and analyzed appropriately considering such spatial correlations. An experimental approach to reproduce such spatial variability similar as numerical realizations in this study is proposed recently and the results show that the mechanical responses of the heterogeneous soils should be understood considering both the local inherent behavior and spatial distributions (Garzón *et al.*, 2015). More explanations and discussions can be found in Kim (2005) and Kim and Santamarina (2008).

### 3. Results – Emergent Phenomena

An emergent phenomenon refers herein to a behavior observed in a spatially varying medium that is not observed in a homogeneous material with the same constitutive law. Emergent phenomena found in this study are discussed next.

#### 3.1 Stress-induced Internal Homogenization of the Stress Field

Spatially correlated heterogeneous specimens are numerically generated and subjected to zero-lateral strain uniaxial loading conditions. At each loading stage, we compute the average in-plane stress  $\sigma_0 = (\sigma_x + \sigma_z)/2$  for each  $i$ -th element, and normalize it by the global average stress applied at the boundaries  $\sigma_{x@b}$  and  $\sigma_{z@b}$ :

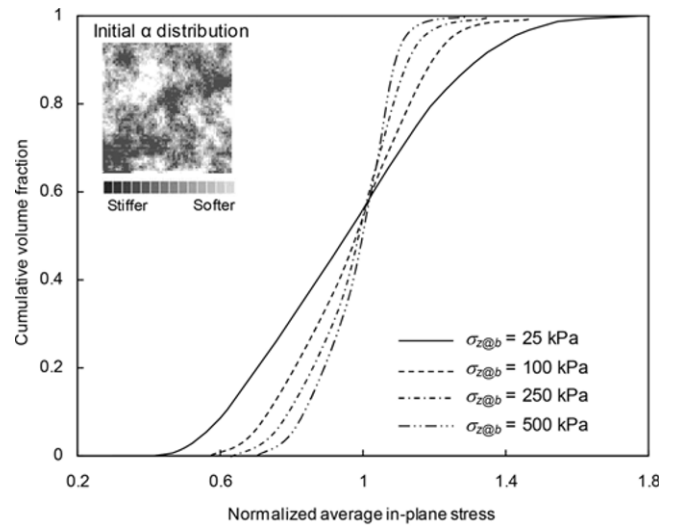


Fig. 1. Distribution of Average In-plane Stress Acting on Mesh Elements, Normalized by the Global Average In-plane Stress Acting at the Boundaries (Equation 7) - Data Shown for one Realization at Different Applied Vertical Loads. Zero-lateral Strain Loading. Spatially Varying Medium with:  $\mu[\alpha] = 10$  MPa,  $\text{COV}[\alpha] = 0.3$ , Relative Correlation Length  $L/D = 0.1$

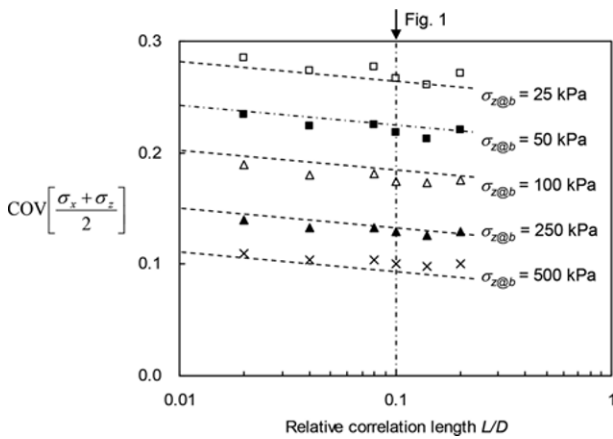


Fig. 2. Coefficient of Variation for Internal Mean Principal Stress Distribution vs. Relative Correlation Length. The Dotted Lines are the Fitted Regression Function in Equation (8). There is one Realization for Each  $L/D$  Value. The Six Realizations are Generated for  $\mu[\alpha] = 10$  MPa and  $COV[\alpha] = 0.3$

$$(\text{Normalized average in - plane stress}) = \frac{(\sigma_x + \sigma_z)_i}{\sigma_{x@b} + \sigma_{z@b}} \quad (7)$$

Cumulative distributions for the normalized average in-plane stress at different loading stages for one realization are shown in Fig. 1. These results suggest that the stress distribution becomes homogenized as the applied vertical stress increases. Furthermore, the probability distribution becomes skewed towards smaller values as softer zones remain shielded by stress arching.

Multiple simulations are conducted with various correlation lengths keeping the other statistics constant (uniform distribution of mean  $\mu[\alpha] = 10$  MPa and coefficient of variation  $COV[\alpha] = 0.3$ ). Results are summarized in Fig. 2. The coefficient of variation for the internal average in-plane stress  $COV[(\sigma_x + \sigma_z)/2]$  is plotted versus the relative correlation length  $L/D$  for different applied vertical stress levels. In all cases, stress distributions become homogenized when the applied vertical stress increases. There is higher homogenization of the stress

field in specimens with high relative correlation length. Dotted lines in Fig. 2 are obtained from a multi-variable regression analysis with two independent input variables: the relative correlation length  $L/D$  and the vertical stress applied at the top boundary  $\sigma_{z@b}$ . The estimated COV for the average in-plane stress is (applicable to simulated conditions only):

$$COV[(\sigma_x + \sigma_z)/2] = 0.43 - 0.007 \ln(L/D) - 0.057 \ln(\sigma_{z@b}/1 \text{ kPa}) \quad (R^2 = 0.98) \quad (8)$$

It can be seen that the coefficient for the applied stress (-0.057) is much greater than the coefficient for the relative correlation length (-0.007); this highlights the importance of confining stress on internal stress homogenization.

### 3.2 Stress Focusing Through Stiffer Zones

Simulations are repeated for correlated heterogeneous media with the same boundary conditions and spatial distribution, but with different variance in the  $\alpha$ -factor that defines the small-strain stiffness:  $COV[\alpha] = 0.1, 0.3,$  and  $0.5$  (see Table 1 – Note: the requirement that  $\alpha$  is positively valued  $\alpha \geq 0$  implies that  $COV[\alpha] \leq 1/\sqrt{3} = 0.57$  for the uniformly distributed  $\alpha$ -factor). Fig. 3 shows the vertical stress distribution under zero-lateral strain loading for an applied vertical load of  $\sigma_{z@b} = 100$  kPa. Black areas correspond to a vertical stress  $\sigma_z \geq 105$  kPa. These results suggest that media with higher stiffness variance experience more pronounced stress concentration towards load-carrying columnar regions even if the spatial distribution of the initial stiffness is isotropic as shown in Fig. 3(a). The emergence of high-stress columnar regions in these meso-scale simulations of spatially varying granular materials resembles the development of load-carrying granular chains in inherently variable discrete element simulations.

Results of a comprehensive study are summarized in Fig. 4. The area ratio that carries a vertical stress  $\sigma_z \geq 105$  kPa when the applied vertical load is  $\sigma_{z@b} = 100$  kPa, is plotted in Fig. 4a as a function of the variance in stiffness for uncorrelated realizations

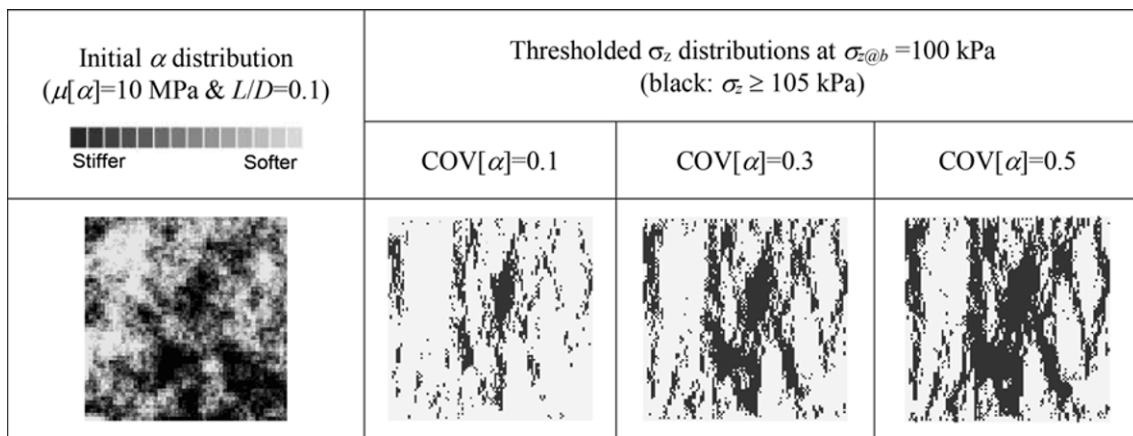


Fig. 3. The Effect of Variability in  $\alpha$  (the Small Strain Shear Modulus at  $\sigma_0 = 1$  kPa) on Local Stress Focusing – Results Show Typical Realizations for Different  $COV[\alpha]$ . Each Realization is a Member of a Set of Monte Carlo Simulations. The Spatial Correlation is  $L/D = 0.1$  in all Cases

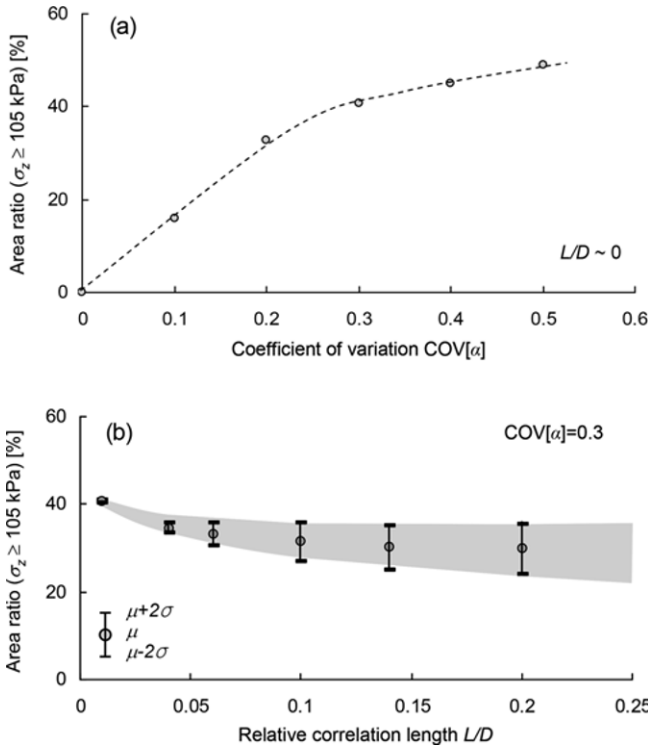


Fig. 4. Vertical Stress Focusing when  $\sigma_{z@b} = 100$  kPa. (a) Area Ratio that Carries Vertical Stress Higher than 105 kPa for Different  $COV[\alpha]$  in Realizations with Short Correlation Length ( $L/D \sim 0$ ); the Two-sigma Range is Much Smaller than the Dot Size used to Indicate the Mean Values. (b) Area Ratio that Carries Vertical Stress Higher than 105 kPa as a Function of Relative Correlation Length for Realizations with  $COV[\alpha] = 0.3$ . One Hundred Realizations are Simulated for Each Case

$L/D \sim 0$  (Note: effectively, the smallest correlation length that can be numerically modeled is determined by the pixel size, hence, in our case  $L/D \geq 1/100$ ). These results show that stress focusing (1) develops even in systems which are uncorrelated, and (2) is enhanced when the variance in initial stiffness increases (as shown in Fig. 3). The effect of relative correlation length  $L/D$  on stress focusing is explored in Fig. 4b ( $\sigma_{z@b} = 100$  kPa,  $COV[\alpha] = 0.3$ ): longer correlation length yields a wider dispersion of internal stress distribution statistics among multiple realizations, and fewer elements appear to carry extra load as  $L/D$  increases. In fact, if the correlation length is infinitely longer than the specimen size  $L/D \gg 1$ , each realization approaches a homogenous medium, and there is no stress focusing.

### 3.3 Reduction and Fluctuation in the Stress Ratio $K_0$

The horizontal stress increases during zero-lateral strain uniaxial compression. In linear elasticity, the ratio of horizontal to vertical stress is related to Poisson's ratio as  $K_0 = \sigma_h/\sigma_v = \nu/(1 + \nu)$ . The meaning of  $K_0$  in granular media can be readily understood with the following mind experiments: (1) a virtual horizontal force is needed to prevent the buckling of vertical

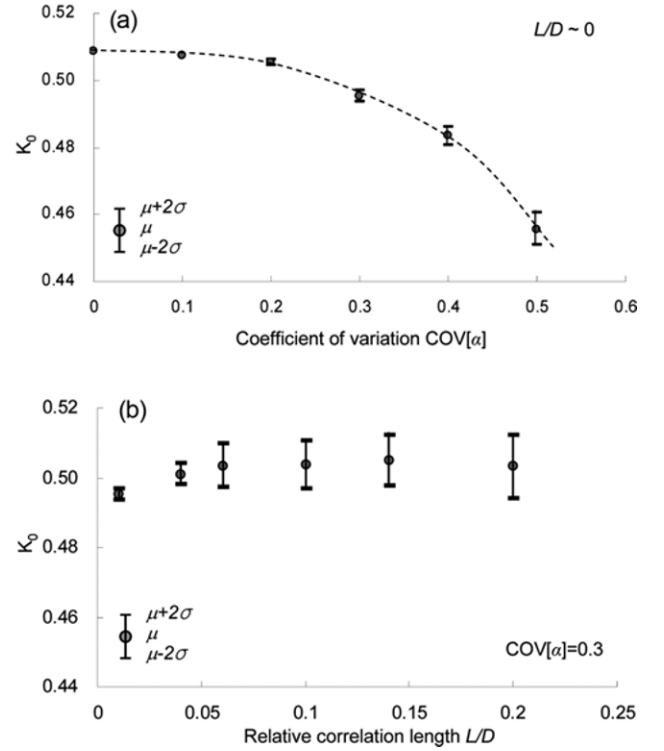


Fig. 5. Horizontal-to-vertical Stress Ratio  $K_0$  when  $\sigma_{z@b} = 100$  kPa. (a)  $K_0$  for Different  $COV[\alpha]$  in Realizations with Short Correlation Length ( $L/D \sim 0$ ). (b)  $K_0$  as a Function of relative Correlation Length for Realizations with  $COV[\alpha] = 0.3$ . One Hundred Realizations are Simulated for Each Case

chains in a perfect simple cubic packing, thus  $K_0 \rightarrow 0$ ; (2) the required lateral force is half the vertical force in an equilateral triangular packing of frictionless monosize particles, i.e.,  $K_0 = 0.5$ ; and (3) the required lateral force will diminish as interparticle friction increases, observed in DEM simulations by Sheng *et al.* (2004). These observations suggest that  $K_0$  in granular materials is fabric and friction dependent.

The effect of meso-scale spatial variability on  $K_0$  in granular materials is evaluated using the results from these numerical simulations. Fig. 5a shows the coefficient of lateral stress at rest  $K_0$  for realizations with short relative correlation length  $L/D \sim 0$  at  $\sigma_{z@b} = 100$  kPa. The data show that the mean value of  $K_0$  decreases and its variance increases with increasing variance in initial stiffness  $COV[\alpha]$ . The effect of relative correlation length on the mean  $K_0$  is less pronounced, as shown in Fig. 5b ( $K_0$  values at  $\sigma_{z@b} = 100$  kPa - fixed  $COV[\alpha] = 0.3$ ); instead, higher correlation length leads to higher variance in  $K_0$ .

When these results are compared to stress focusing trends captured in Figs. 4a and 4b, it is observed that cases with lower stress focusing yield greater mean  $K_0$ , while a wider variance in stress focusing among realizations leads to wider range in  $K_0$  values. Apparently, the load carrying columns that emerge within the medium can effectively transfer the applied vertical load across the specimen and require a smaller lateral confining stress to prevent shear than the homogeneous medium.

### 3.4 Reduced Global Stiffness

The nonlinear load-deformation response for three uncorrelated realizations  $L/D \sim 0$  with different coefficients of variation in the initial stiffness distribution  $COV[\alpha]$  are shown in Fig. 6. Greater compressibility is observed for higher variance in stiffness distribution, in agreement with published results gathered with elastic models reviewed earlier.

The evolution of the global constrained modulus with applied vertical stress for different initial stiffness variance  $COV[\alpha]$  is shown in Fig. 7, with emphasis on realizations with the same correlation length  $L/D = 0.2$ . For clarity, the secant constrained modulus for the heterogeneous medium  $M_{hetero}$  is normalized by the secant constrained modulus for

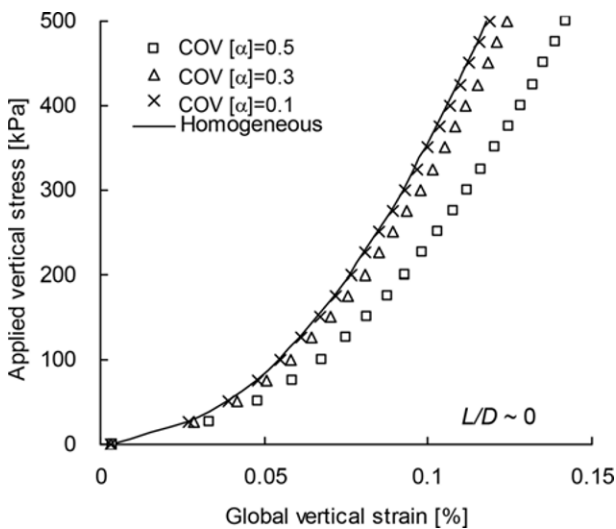


Fig. 6. Stress-strain Curves under  $K_0$  Loading Conditions Obtained for four Realizations with Different Variance in Initial Stiffness and Uncorrelated Spatial Distribution

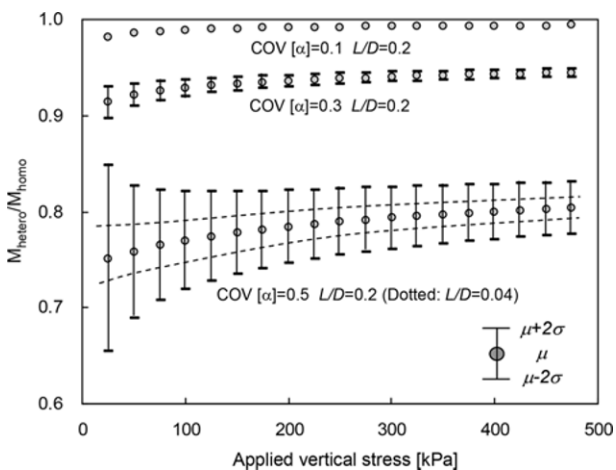


Fig. 7. Normalized Tangential Constraint Modulus  $M_{hetero}/M_{homo}$  Versus Applied Vertical Stress. The Two-sigma Range is Estimated from Twenty Realizations Run for Each Case. The Two-sigma Range for the Case of  $COV[\alpha] = 0.1$  and  $L/D = 0.2$  is much Smaller than the Dot Size used to Indicate the Mean Values ( $COV[M_{hetero}/M_{homo}] < 0.01$ )

the homogeneous medium  $M_{homo}$  at the same stress level. Results show that

- As stiffness variance  $COV[\alpha]$  increases, the global constrained  $M$  decreases; for example, a heterogeneity of  $COV[\alpha] = 0.5$  causes a 25% decrease in the effective stiffness at  $\sigma_{z@b} = 25$  kPa compared to the homogeneous medium with stiffness equal to the arithmetic mean  $\mu[\alpha]$ .
- As stiffness variance  $COV[\alpha]$  increases, the constrained modulus becomes more stress-dependent, i.e., higher rate of change with increasing applied vertical stress.
- The relative correlation length  $L/D$  has a small effect on the expectation of the global constrained modulus: Differences between the mean  $M_{hetero}/M_{homo}$  for media with  $L/D = 0.04$  and  $L/D = 0.2$  are less than 5% even for  $COV[\alpha] = 0.5$ . However, the correlation length determines the variance of the computed effective constrained modulus among realizations. Note: these two observations are analogous to published results based on linear elastic models (Beacher and Ingra, 1981; Zeitoun and Baker, 1992; Paice *et al.*, 1996).
- There is a gradual increase in  $M_{hetero}/M_{homo}$  and a decrease in  $COV[M_{hetero}/M_{homo}]$  with the increase in applied vertical stress. Both trends are consequences of stress-induced homogenization.

### 4. Conclusions

Spatially varying small-strain stiffness is anticipated in granular materials. Meso-scale simulations using a stress-dependent nonlinear granular material model show that:

1. The global stiffness decreases and becomes more sensitive to stress changes as the variability in internal stiffness increases.
2. A wider range in global stiffness is anticipated for longer correlation lengths.
3. Spatially varying stiffness causes a non-homogeneous stress field inside the granular mass, and load transfer focuses along columnar zones.
4. Columnar stress focusing implies higher stress anisotropy; in other words, the horizontal-to vertical stress ratio  $K_0$  is lower for heterogeneous granular media.
5. The internal stress field tends to homogenize as the confining stress increases due to the inherent stress-dependent response of granular materials.

### Acknowledgements

This research was supported by a grant on Scale Effects in Soils from the National Science Foundation and on Hydrates from the Department of Energy and a grant (13SCIPS04) from Smart Civil Infrastructure Research Program funded by Ministry of Land, Infrastructure and Transport (MOLIT) of Korea government and Korea Agency for Infrastructure Technology Advancement (KAIA).

## References

- ABAQUS/Standard User's Manual, Version 6.6 (2007). Pawtucket: Habbitt, Karlsson & Sorenson, Inc..
- Ang, A. H. S. and Tang, W. H. (1975). *Probability concept in engineering planning and design*, Vol. 1. New York: Wiley and Sons.
- Antonellini, M. A., Aydin, A., and Pollard, D. D. (1994). "Microstructure of deformation bands in porous sandstones at Arches National Park, Utah." *Journal of Structural Geology*, Vol. 16, pp. 941-959.
- Antonellini, M. A., Aydin, A., Pollard, D. D., and D'Onfro, P. (1994). "Petrophysical study of faults in sandstones using petrographic image analysis and X-ray computerized tomography." *Pure and Applied Geophysics*, Vol. 143, pp. 181-201.
- Arévalo, R., Zuriguel, I., and Maza, D. (2009). "Topological properties of the contact network of granular materials." *International Journal of Bifurcation and Chaos*, Vol. 19, pp. 695-702.
- Barreto, D. and O'Sullivan, C. (2012). "The influence of interparticle friction and the intermediate stress ratio on soil response under generalised stress conditions." *Granular Matter*, Vol. 14, No. 4, pp. 505-521.
- Beacher, G. B. and Ingra, T. S. (1981). "Stochastic FEM in settlement predictions." *ASCE Journal of Soil Mechanics and Foundation Division*, Vol. 107, No. 4, pp. 449-463.
- Behringer, R., Daniels, K. E., Majmudar, T. S., and Sperl, M. (2008). "Fluctuations, correlations, and transitions in granular materials: Statistical mechanics for a non-conventional system." *Philosophical Transactions of the Royal Society A*, Vol. 366, No. 1865, pp. 493-504.
- Cambou, B. (1975). "Applications of first-order uncertainty analysis in the finite elements method in linear elasticity." *Proc. Applications of Statistics and Probability in Soil and Structure Engineering*, 2nd International Conference, Aachen, Germany, pp. 117-122.
- Ching, J. and Phoon, K. K. (2013). "Effect of element sizes in random field finite element simulations of soil shear strength." *Computers and Structures*, Vol. 126, No. 15, pp. 120-134.
- Ching, J. and Phoon, K. K. (2013). "Mobilized shear strength of spatially variable soils under simple stress states." *Structural Safety*, Vol. 41, pp. 20-28.
- Cho, G. C., Lee, J. S., and Santamarina, J. C. (2004). "Spatial variability in soils: high resolution assessment with electrical needle probe." *ASCE Journal of Geotechnical and Geoenvironmental Engineering*, Vol. 130, No. 8, pp. 843-850.
- Cundall, P. A. and Strack, O. D. L. (1979). "A discrete numerical model for granular assemblies." *Geotechnique*, Vol. 29, pp. 47-65.
- DeGroot, D. J. (1996). "Analyzing spatial variability of in-situ soil properties." *Proc. Uncertainty '96, Madison*, pp. 210-238.
- DeGroot, D. J. and Beacher, G. B. (1993). "Estimating autocovariance of in-situ soil properties." *ASCE Journal of Geotechnical Engineering*, Vol. 119, No. 1, pp. 147-166.
- Díaz-Rodríguez, J. A. and Santamarina, J. C. (1999). "Thixotropy: The Case of Mexico City Soils." *XI Panamerican Conference on Soil Mechanics and Geotechnical Engineering, Iguazu Falls, Brazil*, Vol. 1, pp. 441-448.
- Duncan, J. M. and Chang, C. Y. (1970). "Nonlinear analysis of stress and strain in soils." *ASCE Journal of the Soil Mechanics and Foundations Division*, Vol. 96, No. 5, pp. 1629-1653.
- El-Kadi, A. I. and Williams, S. A. (2000). "Generating two-dimensional fields of auto-correlated, normally distributed parameters by the matrix decomposition technique." *Ground Water*, Vol. 38, No. 4, pp. 530-532.
- f settlement prediction—case history." *Journal of Wu, T. H., Gale, S. M., Zhou, S. Z., and Geiger, E. C. (2011). "Reliability of Geotechnical and Geoenvironmental Engineering*, Vol. 137, No. 4, pp. 312-322.
- Fenton, G. A. (1994). "Error evaluation of three random field generators." *ASCE Journal of Engineering Mechanics*, Vol. 120, No. 12, pp. 2478-2497.
- Fenton, G. A. and Griffiths, D. V. (2005). "Three-dimensional probabilistic foundation settlement." *ASCE Journal of Geotechnical and Geoenvironmental Engineering*, Vol. 131, No. 2, pp. 232-239.
- Fenton, G. A. and Griffiths, D. V. (2008). *Risk assessment in geotechnical engineering*, New York: John Wiley and Sons.
- Fernandez, A. L. (2000). *Tomographic imaging the state of stress*, PhD Thesis, Georgia Institute of Technology.
- Garzón, L. X., Caicedo, B., Sánchez-Silva, M., and Phoon, K. K. (2015). "Physical modelling of soil uncertainty." *International Journal of Physical Modelling in Geotechnics*, Vol. 15, Issue 1, pp. 19-34.
- Griffiths, D. V. and Fenton, G. A. (2009). "Probabilistic settlement analysis by stochastic and random finite-element methods." *Journal of Geotechnical and Geoenvironmental Engineering*, Vol. 135, No. 11, pp. 1629-1637.
- Grigoriu, M. (1984). "Crossing of non-Gaussian translation process." *ASCE Journal of Engineering Mechanics*, Vol. 110, No. 4, pp. 610-620.
- Harr, M. E. (1987). *Reliability based design in civil engineering*, New York: McGraw Hill, London.
- Hegazy, A. H., Mayne, P. M., and Rouhani, S. (1996). "Geostatistical assessment of spatial variability in piezocone tests." *Proc. Uncertainty '96, Madison*, pp. 254-268.
- Huang, J. and Griffiths, D. V. (2015). "Determining an appropriate finite element size for modelling the strength of undrained random soils." *Computers and Geotechnics*, Vol. 69, pp. 506-513.
- Huang, J., Griffiths, D. V., and Fenton G. A. (2010). "Probabilistic Analysis of Coupled Soil Consolidation." *Journal of Geotechnical and Geoenvironmental Engineering*, Vol. 136, No. 3, pp. 417-430.
- Hurley, R., Marteau, E., Ravichandran, G., and Andrade, J. E. (2014). "Extracting inter-particle forces in opaque granular materials: Beyond photoelasticity." *Journal of the Mechanics and Physics of Solids*, Vol. 63, pp. 154-166.
- Jang, D. J., Frost, J. D., and Park, J. Y. (1999). "Preparation of epoxy impregnated sand coupons for image analysis." *ASTM Geotechnical Testing Journal*, Vol. 22, No. 2, pp. 147-158.
- Jimenez, R. and Sitar, N. (2009). "The importance of distribution types on finite element analyses of foundation settlement." *Computers and Geotechnics*, Vol. 36, pp. 474-483.
- Jones, A. L., Kramer, S. L., and Arduino, P. (2002). *Estimation of uncertainty in geotechnical properties for performance-based earthquake engineering*, PEER report 2002/16.
- Kulhawy, F. H. (1992). "On evaluation of static soil properties." *Stability and Performance of Slopes and Embankments II (GSP 31)*, New York, pp. 95-115.
- Lacasse, S. and Nadim, F. (1996). "Uncertainties in characterizing soil properties." *Proc. Uncertainty '96, Madison*, pp. 49-75.
- Majmudar, T. S. and Behringer, R. P. (2005). "Contact force measurements and stress-induced anisotropy in granular materials." *Nature*, Vol. 435, pp. 1079-1082.
- Muthuswamy, M. and Tordesillas, A. (2006). "How do interparticle friction, packing density and degree of polydispersity affect force propagation in particulate assemblies?" *Journal of Statistical Mechanics: Theory and Experiment* (opscience.iop.org/1742-5468/2006/09/P09003)
- Niemunis, A., Wichtmann, T., Petryna, Y., and Triantafyllidis, T. (2005).

- “Stochastic modelling of settlements due to cyclic loading for soil-structure interaction.” *Proc. the 9th International Conference on Structural Safety and Reliability*, ICOSAR’05, Rome, Italy. Rotterdam, Millpress.
- Oda, M., Takemura, T., and Takahashi, M. (2004) “Microstructure in shear band observed by microfocus X-ray computed tomography.” *Geotechnique*, Vol. 54, No. 8, pp. 539-542.
- Paice, G. M., Griffiths, D. V., and Fenton, G. A. (1996). “Finite element modeling of settlements on spatially random soil.” *ASCE Journal of Geotechnical and Geoenvironmental Engineering*, Vol. 122, No. 9, pp. 777-779.
- Peña, A. A., Hermann, H. J., and Lind, P. G. (2009). “Force chains in sheared granular media of irregular particles.” *Powders and Grains 2009 AIP Conference Proceedings*, Proceedings of the Sixth International Conference Micromechanics of Granular Media 2009, Colorado, USA., pp. 321-324.
- Phoon, K. K. and Kulhawy, F. H. (1999). “Characterization of geotechnical variability.” *Canadian Geotechnical Journal*, Vol. 36, pp. 612-624.
- Radjai, F., Wolf, D. E., Jean, M., and Moreau, J. J. (1998). “Bimodal character of stress transmission in granular packings,” *Physical Review Letters*, Vol. 80, pp. 61-64.
- Ravi, V. (1992). “Statistical modeling of spatial variability of undrained strength.” *Canadian Geotechnical Journal*, Vol. 29, pp. 721-729.
- Resendiz, D. and Herrera, I. (1969). “A probabilistic formulation of settlement control design.” *Proc. 7th ICSMFE*, Vol. 2, Mexico, pp. 217-225.
- Rothenburg, L. and Bathurst, R. J. (1989). “Analytical study of induced anisotropy in idealized granular materials.” *Geotechnique*, Vol. 39, No. 4, pp. 601-614.
- Santamarina, J. C., Klein, K. A., and Fam, M. A. (2001). *Soils and waves*, New York: John Wiley and Sons.
- Santoso, A. M., Phoon, K. K., and Quek, S.-T. (2011). “Effects of soil spatial variability in rainfall-induced landslides.” *Computers and Structures*, Vol. 89, Nos. 11-12, pp. 893-900.
- Sheng, Y., Lawrence, C. J., Briscoe, B. J., and Thornton, C. (2004). “Numerical studies of uniaxial powder compaction process by 3D DEM.” *Engineering Computations*, Vol. 21, pp. 304-317.
- Song, K.-I., Cho, G. C., and Lee, S. W. (2011). “Effects of spatially variable weathered rock properties on tunnel behavior.” *Probabilistic Engineering Mechanics* Vol. 26, No. 3, pp. 413-426.
- Suchomel, R. and Masin, D. (2011). “Probabilistic analyses of a strip footing on horizontally stratified sandy deposit using advanced constitutive model.” *Computers and Geotechnics*, Vol. 38, pp. 363-374
- Tang, W. (1979). “Probabilistic evaluation of penetration resistance.” *ASCE Journal of Geotechnical Engineering*, Vol. 105, No. 10, pp. 1173-1191.
- Tordesillas, A., O’Sullivan, P., and Walker, D. M. (2010). “Paramitha Evolution of functional connectivity in contact and force chain networks: Feature vectors, k-cores and minimal cycles.” *Comptes Rendus Mécanique*, Vol. 338, pp. 556-569.
- Vanmarcke, E. H. (1977). “Probabilistic modeling of soil profiles.” *Journal of the Soil Mechanics and Foundation Division, ASCE*, Vol. 103, No. 11, pp. 1227-1246.
- Vio, R., Andreani, P., and Wamsteker, W. (2001). “Numerical simulation of non-Gaussian random fields with prescribed correlation structure.” *The Astronomical Society of the Pacific*, Vol. 113, pp. 1009-1020.
- Yamazaki, F. and Shinozuka, M. (1988). “Digital generation of non-Gaussian stochastic fields.” *ASCE Journal of Engineering Mechanics*, Vol. 114, No. 7, pp. 1183-1197.
- Zeitoun, D. G. and Baker, R. (1992). “A stochastic approach for settlement predictions of shallow foundations.” *Geotechnique*, Vol. 42, No. 4, pp. 617-629.